



## Original Article

# Effect of Annealing Temperatures on Structural and Luminescence Properties of SnO<sub>2</sub> Nanoparticles

Trinh Thi Loan\*, Vu Hoang Huong

*VNU University of Science, 334 Nguyen Trai, Thanh Xuan, Hanoi, Vietnam*

Received 6<sup>th</sup> June 2025

Revised 21<sup>st</sup> June 2025; Accepted 30<sup>th</sup> September 2025

**Abstract:** The aim of this work is to reveal the structural and photoluminescence properties of SnO<sub>2</sub> synthesized via facile sol-gel method by systematically varying annealing temperatures. X-ray diffraction (XRD) analysis showed that all samples possess a polycrystalline single-phase tetragonal rutile structure without impurities. Both the crystallite size and crystalline quality of the samples increase with rising annealing temperatures. Raman spectroscopy demonstrated the presence of forbidden Raman and IR-active modes in SnO<sub>2</sub> nanoparticles. Both the positions and intensities of the Raman peaks are significantly influenced by annealing temperatures, which correlate with variations in crystallite size and crystalline quality of the synthesized materials. Additionally, photoluminescence (PL) spectra exhibited peaks in both the ultraviolet (UV) and visible regions. The UV emission peaks arise from electron recombination near the band gap, while the visible emission peaks are attributed to oxygen vacancies ( $V_O^0, V_O^+, V_O^{++}$ ) and tin interstitials. This research provides valuable foundational knowledge that will support future studies on SnO<sub>2</sub>.

**Keywords:** Sol-gel, SnO<sub>2</sub> nanoparticles, annealing temperature, Raman, luminescence.

## 1. Introduction

In recent years, many researchers have focused on synthesizing SnO<sub>2</sub> nanomaterials in various sizes and shapes to investigate their unique properties [1]. Tin dioxide is widely studied because it is chemically stable, transparent to light, and possible well to electrically conduct when it is doped by Fluorine (F) [2, 3]. These properties make SnO<sub>2</sub> useful in several applications, including batteries [4], dye-sensitized solar cells [5], photocatalysis [6], transparent electrodes [7], and gas sensors [8]. The properties of SnO<sub>2</sub>, such as band gap, crystal structure, morphology, and defects, can be tailored by

\* Corresponding author.

E-mail address: loan.trinhthi@gmail.com

adjusting the synthesis conditions, including temperature, precursor materials, and solvents used [9]. In this work,  $\text{SnO}_2$  nanoparticles were synthesized by sol–gel method using  $\text{SnCl}_2$  as precursor materials, without adding any capping agents or surfactants. We investigated how the size of the nanoparticles affects their light emission properties. Understanding these photoluminescence properties helps us to learn more about the optical behavior of  $\text{SnO}_2$  nanomaterials and improves their use in optical devices. The obtained results provide important foundational knowledge of nano  $\text{SnO}_2$  for the future research and applications in various technological fields.

## 2. Experimental

$\text{SnO}_2$  nanoparticles were synthesized using sol–gel method. The precursor,  $\text{SnCl}_2 \cdot 2\text{H}_2\text{O}$  was dissolved in 30 mL  $\text{C}_2\text{H}_5\text{OH}$  with continuously stirring. Next, the 10 ml ethylene glycol was added to the mixture solution under vigorous stirring. Then the solution was heated at 100 °C during stirring till getting a transparent gel, next it was dried at 100 °C for 24 h. The dried product was annealed at temperatures of 400, 600, 800 and 1,100 °C for 3 h.

The crystalline structure of  $\text{SnO}_2$  nanoparticles was studied on an Empyrean X-ray diffractometer (XRD), using  $\text{Cu-K}_{\alpha 1}$  irradiation ( $\lambda = 1.54056 \text{ \AA}$ ). Raman spectra were obtained using a micro-Raman spectrophotometer LabRAM HR 800 (HORIBA JobinYvon) with a 632.8 nm excited wavelength. The morphologies of the samples were examined using a transmission electron microscope (TEM, JEOL/JEM 1010). Photoluminescence (PL) and photoluminescence excitation (PLE) spectra were recorded at room temperature using a Fluorolog FL3-22 spectrofluorometer (Jobin Yvon Spex) with a 450 W xenon lamp as the excitation source.

## 3. Results and Discussion

### 3.1. Structure Characterization

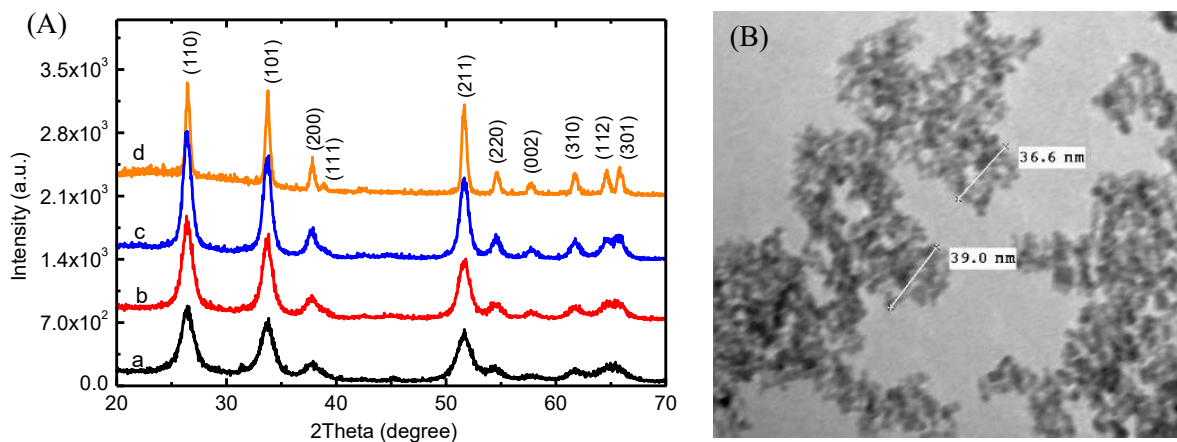


Figure 1. (A) XRD patterns of  $\text{SnO}_2$  samples at different annealing temperatures: a- 400 °C, b- 600 °C, c- 800 °C, d- 1,100 °C; (B) FESEM image of  $\text{SnO}_2$  sample annealed at 600 °C.

XRD patterns of  $\text{SnO}_2$  samples annealed at temperatures of 400, 600, 800 and 1,100 °C are presented in Fig. 1 (A). All the samples have characteristic XRD peaks of (110), (101), (200), (111), (211), (220),

(002), (310), (112), and (301) crystalline planes of the tetragonal rutile structure with the space group  $D_{4h}14$  ( $P4_2/mnm$ ), as referenced in JCPDS No. 21-1250. The positions of the diffraction peaks remain almost unchanged across different annealing temperatures, this indicates that the crystalline structure of  $\text{SnO}_2$  is stable under elevated temperatures. However, the intensity and sharpness of the peaks increase gradually with increasing annealing temperatures. This enhancement is explained due to the increase in crystallite size, which is attributed to thermally promoted crystallite growth and a reduction in specific surface area. The grain size of the crystallites and inter-planer spacing (d-value) were calculated based on Scherer's and Bragg's equations:

$$D = \frac{k\lambda}{\beta \cos\theta} [10] \text{ and } d = \frac{\lambda}{2\sin\theta} [11]$$

where  $D$  is the mean crystallite size,  $K$  is the shape factor taken as 0.89,  $\lambda$  is the wavelength of the incident beam,  $\beta$  is the full width at half maximum and  $\theta$  is the Bragg angle. These results are shown in Table 1.

Table 1. XRD parameters and size of  $\text{SnO}_2$  nanoparticles at different annealing temperatures.

Annealing temperature (°C)	2θ (°)	d- spacing (Å)	FWHM (°)	Crystallite size (nm)	Average crystalline size D (nm)
400	26.44	3.3687	1.2232	6.7	6.7
	33.70	2.6574	1.1681	7.1	
	51.67	1.7676	1.3842	6.4	
600	26.44	3.3683	1.0379	7.9	8.4
	33.71	2.6565	0.96572	8.6	
	51.65	1.7682	1.0200	8.7	
800	26.43	3.3701	0.82288	9.9	10.4
	33.72	2.6558	0.78625	10.6	
	51.65	1.7681	0.82315	10.7	
1100	26.48	3.3635	0.38631	21.1	20.3
	33.75	2.6536	0.40635	20.4	
	51.65	1.7679	0.44148	20.0	

Annealing at temperatures of 400 °C, 600 °C, 800 °C, and 1,100 °C resulted in grain sizes with an average value of 6.7, 8.4, 10.4 and 20.3 nm, respectively. Fig. 1 (B) shows a typical TEM image of  $\text{SnO}_2$  sample annealed at 600 °C. The TEM image depicts the irregular aggregated morphology. The  $\text{SnO}_2$  nanoparticles are polyhedral or irregular in shape. The optimal annealing condition for  $\text{SnO}_2$  samples depends on the desired application. For photocatalytic applications, smaller particle sizes are generally preferred because their effective surface area for reactions increases, thus the photocatalytic activity is enhanced. Thus, an annealing temperature range of 400 °C to 800 °C may be suitable.

Raman scattering is a useful technique for characterizing nanomaterials and identifying lattice defects in the materials [12]. Fig. 2 shows the room temperature Raman spectra from 170  $\text{cm}^{-1}$  to 900  $\text{cm}^{-1}$  of  $\text{SnO}_2$  nanoparticles annealed at different temperatures. The positions and intensities of the Raman peaks vary significantly with annealing temperature. Notably, the intensity of the peak around 634  $\text{cm}^{-1}$  increases rapidly as the annealing temperature rises. These changes may be related to the crystallite size and the crystalline quality of the synthesized  $\text{SnO}_2$  [13]. Annealing at 1,100 °C, the Raman spectrum of the sample exhibits nine peaks at 228, 259, 475, 506, 546, 634, 695, 776, and 866  $\text{cm}^{-1}$ , with the strongest peak at 634  $\text{cm}^{-1}$  (Fig. 2A). The peaks at 475, 634, and 776  $\text{cm}^{-1}$  correspond to the  $E_g$ ,  $A_{1g}$ , and  $B_{2g}$  vibration modes, respectively, consistent with the rutile phase of  $\text{SnO}_2$  [14]. The  $A_{1g}$  and  $B_{2g}$  modes are associated with the expansion and contraction of Sn-O bonds, while the  $E_g$  mode relates to oxygen vibrations within the oxygen plane [14]. Additionally, the peaks at 228 and 259  $\text{cm}^{-1}$

may correspond to the  $E_{u(1)}$ (TO) and  $E_{u(1)}$ (LO) modes, where TO stands for transverse optical phonons and LO stands for longitudinal optical phonons [15, 16]. The peaks at  $506$  and  $695\text{ cm}^{-1}$  may be attributed to the  $A_{2u}$ (TO) and  $A_{2u}$ (LO) modes, respectively [17]. The peak at  $546\text{ cm}^{-1}$  may correspond to the  $B_{1u}$  mode [17], and the peak at  $866\text{ cm}^{-1}$  is likely related to surface defects in the  $\text{SnO}_2$  nanocrystals [18,19]. In contrast, samples annealed at  $600\text{ }^{\circ}\text{C}$  and  $800\text{ }^{\circ}\text{C}$  exhibit six peaks at  $475\text{ cm}^{-1}$  ( $E_g$ ),  $634\text{ cm}^{-1}$  ( $A_{1g}$ ),  $774\text{ cm}^{-1}$  ( $B_{2g}$ ),  $253\text{ cm}^{-1}$  ( $E_{u(1)}$ (LO)),  $301\text{ cm}^{-1}$  ( $E_{u(2)}$ (LO)) [15, 16], and  $571\text{ cm}^{-1}$  ( $A_{2g}$ ) [20] (Fig 2, B and C). At the lowest annealing temperature of  $400\text{ }^{\circ}\text{C}$ , the Raman spectrum shows seven broad and weak peaks at approximately  $218$ ,  $268$ ,  $411$ ,  $537$ ,  $638$ ,  $758$ , and  $870\text{ cm}^{-1}$ .

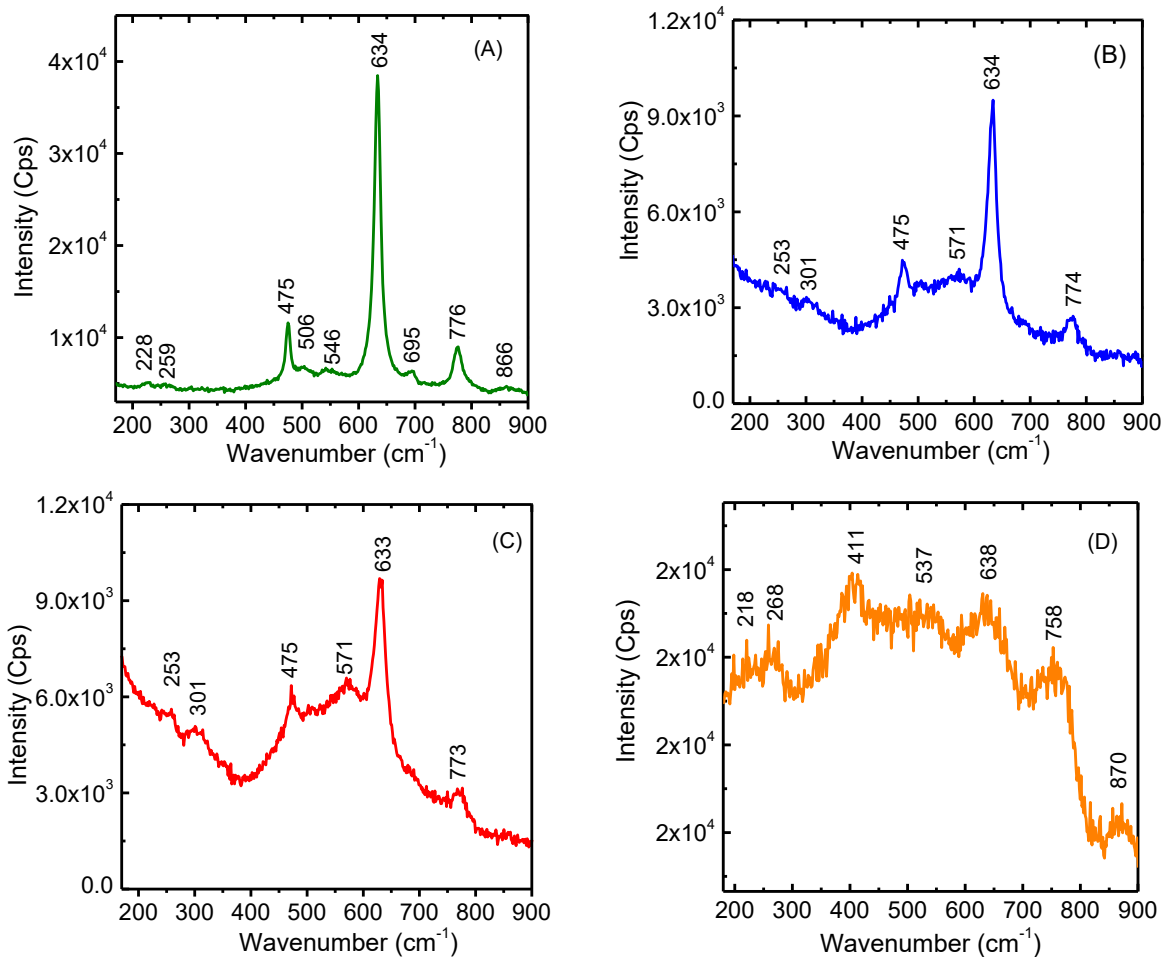


Figure 2. Raman spectra of  $\text{SnO}_2$  samples at different annealing temperatures:  
A-  $1100\text{ }^{\circ}\text{C}$ , B-  $800\text{ }^{\circ}\text{C}$ , C-  $600\text{ }^{\circ}\text{C}$ , D-  $400\text{ }^{\circ}\text{C}$ .

The peaks at  $218$ ,  $268$ , and  $758\text{ cm}^{-1}$  are attributed to the  $E_{u(1)}$ (TO),  $E_{u(2)}$ (LO), and  $E_{u(3)}$ (LO) vibrational modes of  $\text{SnO}_2$ , respectively [21]. The peaks at  $411$  and  $537\text{ cm}^{-1}$  correspond to the  $A_{2g}$  [12] and  $B_{1u}$  [17] vibration modes. The peak at  $638\text{ cm}^{-1}$  is attributed to the  $A_{1g}$  symmetric Sn–O stretching mode in nanocrystalline  $\text{SnO}_2$ , and the peak at  $870\text{ cm}^{-1}$  is associated with surface defects [18, 19]. It is well known that the  $A_{2u}$  and  $E_u$  modes are IR-active, while the  $A_{2g}$  and  $B_{1u}$  modes are Raman-silent [13-19]. The presence of forbidden Raman modes ( $A_{2g}$ ,  $B_{1u}$ ) and IR-active modes ( $A_{2u}$ ,  $E_u$ ) in the samples

can be attributed due to changes in bond lengths, reduced space symmetry, lattice distortions caused by oxygen vacancies, and local lattice disorders in the  $\text{SnO}_2$  nanoparticles [19].

### 3.2. Optical Characterization

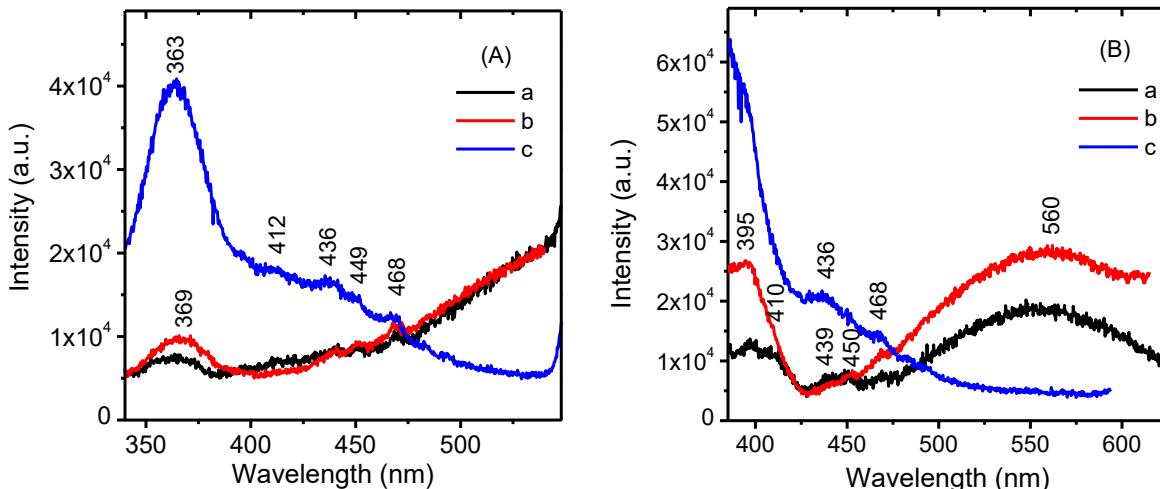


Figure 3. PL spectra under excitation wavelengths of (A) 300 nm and (B) 335 nm of the samples annealed at (a) 400 °C, (b) 800 °C and (c) 1100 °C.

Photoluminescence (PL) spectroscopy is a highly sensitive and effective technique for studying charge carrier recombination, trapping, and defects within materials. In  $\text{SnO}_2$  nanoparticles, the most energetically favourable intrinsic defects are oxygen vacancies and tin interstitials. Tin interstitials are located within the conduction band, while oxygen vacancies exist in the band gap region [16]. PL spectra were recorded at two excitation wavelengths,  $\lambda_{\text{ex}} = 300$  nm and  $\lambda_{\text{ex}} = 335$  nm, for samples annealed at different temperatures, as shown in Figs 3A and 3B, respectively. When excited at  $\lambda_{\text{ex}} = 300$  nm, the sample annealed at 1,100 °C exhibited a strong emission peak at 363 nm (3.42 eV) and four weaker peaks at 412 nm (3.01 eV), 436 nm (2.84 eV), 449 nm (2.76 eV), and 468 nm (2.65 eV). The samples annealed at 400 °C and 800 °C showed similar emission peaks but with significantly lower intensities compared to the sample annealed at 1,100 °C. When excited at  $\lambda_{\text{ex}} = 335$  nm, all samples displayed a new emission peak at approximately 395 nm (3.14 eV). Additionally, the samples annealed at 400 °C and 800 °C showed a broad emission band centred around 560 nm (2.21 eV). Emission peaks observed at 363 nm and 369 nm have energies lower than the band gap of  $\text{SnO}_2$ , indicating that these emissions are not due to the direct recombination of electrons in the conduction band with holes in the valence band. Instead, they are attributed to near-band edge (NBE) transitions resulting from the radiative recombination of electrons and holes [22]. The emission peak at 395 nm originated from the combination of the electron in the conduction band and the hole in the  $V_O^{++}$  (oxygen vacancy has not captured any electron) [23]. Another emission peak at 412 nm/410 nm was attributed to the  $V_O^0$  (which has captured two electrons and is neutral to the lattice) [24]. The emission peak at 436 nm was attributed to the Sn interstitials [24]. The peak at 449 nm might be attributed to the transitions from the various levels of shallow donor states  $V_O^0$  to acceptor level [16]. The peak at 468 nm was attributed to the  $V_O^+$  (which has captured a single electron) [25]. Finally, the broad peak at 560 nm might be originating because of the transitions from the shallow donor levels of  $V_O^0$  to the surface states and  $V_O^+$  levels [16].

The PL spectra of the sample annealed at 800 °C were systematically examined under excitation wavelengths of 280 nm, 300 nm, 310 nm, 324 nm, and 335 nm (Fig. 4). Visible emission peaks at approximately 395 nm, 440 nm, 450 nm, and 468 nm, along with a broad peak around 560 nm, were consistently observed across all excitation wavelengths, with their intensities increasing as the excitation wavelength increased, aligning with previous studies on SnO<sub>2</sub> nanomaterials [23]. Additionally, the ultraviolet (UV) emission peaks shifted to longer wavelengths with higher excitation wavelengths, likely due to varying contributions from NBE emissions and their phonon replicas, resulting from recombination involving energy levels near the band gap [22, 25].

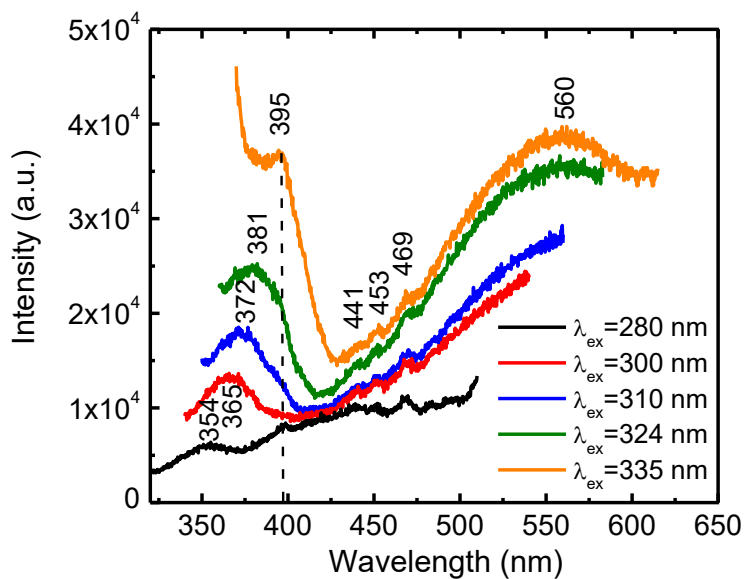


Figure 4. The excitation wavelength-dependent emission spectra of the samples annealed at 800 °C.

#### 4. Conclusion

SnO<sub>2</sub> nanoparticles were successfully synthesized using simple sol–gel method. We investigated the effect of annealing temperature on the crystalline structure and the origin of luminescence peaks in SnO<sub>2</sub> nanoparticles. XRD analysis revealed that all samples are polycrystalline, with diffraction lines corresponding to the rutile phase of SnO<sub>2</sub>. Both the crystallite size and crystal quality of the samples increased when annealing temperatures increased. These improvements in crystallite size and quality significantly enhanced the intensity of the A<sub>1g</sub> vibration mode. Furthermore, some forbidden Raman and IR-active modes, such as A<sub>2g</sub>, B<sub>1u</sub>, A<sub>2u</sub>, and E<sub>u</sub>, which are inactive in bulk samples, became active in the SnO<sub>2</sub> nanoparticles. PL spectra exhibited peaks in both the UV and visible regions. Visible emission peaks correspond to the V<sub>O</sub><sup>0</sup>, V<sub>O</sub><sup>+</sup>, V<sub>O</sub><sup>++</sup> and the Sn interstitials in SnO<sub>2</sub> nanoparticles. The existence of oxygen vacancies and Sn interstitials in the sample annealed at temperatures of 400 °C to 800 °C creates the defect energy levels within the band gap, effectively reducing the energy required for electrons to transition across the gap. This phenomenon can improve the material's solar light absorption and utilization. This research provides valuable foundational knowledge of SnO<sub>2</sub> that would be useful for further studies.

## References

- [1] I. E. Kolesnikov, D. S. Kolokolov, M. A. Kurochkin, M. A. Voznesenskiy, M. G. Osmolowsky, E. Lähderanta, O. M. Osmolovskaya, Morphology and Doping Concentration Effect on the Luminescence Properties of  $\text{SnO}_2:\text{Eu}^{3+}$  nanoparticles, *J. Alloys Compd.*, Vol. 822, No. 15340, 2020, <https://doi.org/10.1016/j.jallcom.2020.153640>.
- [2] D. Toloman, A. Popa, M. Stefan, T. D. Silipas, R. C. Suci, L. B. Tudoran, O. Pana, Enhanced Photocatalytic Activity of Co Doped  $\text{SnO}_2$  Nanoparticles by Controlling the Oxygen Vacancy States, *Optical Materials*, Vol. 110, No. 110472, 2020, <https://doi.org/10.1016/j.optmat.2020.110472>.
- [3] A. Wang, K. Bushick, N. Pant, W. Lee, X. Zhang, J. Leveillee, F. Giustino, S. Poncé, E. Kioupakis, Electron Mobility of  $\text{SnO}_2$  from First Principles, *Appl. Phys. Lett.*, Vol. 124, No. 172103, 2024, <https://doi.org/10.1063/5.0198885>.
- [4] Y. Kong, Z. Ma, Y. Ye, G. He, Y. Sun, X. Zuo, X. Xiao, and J. Nan, Nanosized Amorphous  $\text{SnO}_2$  Particles Anchored in the Wheat Straw Carbon Substrate as the Stabilized Anode Material of Lithium-Ion Batteries, *ACS Appl. Energy Mater.*, Vol. 1, No. 12, 2018, pp. 7065-7075, <https://doi.org/10.1021/acsaelm.8b01408>.
- [5] N. N. Dinh, M. C. Bernard, A. H. Goff, T. Stergiopoulos, P. Falaras, Photoelectrochemical Solar Cells Based on  $\text{SnO}_2$  Nanocrystalline Films, *C.R. Chimie*, Vol. 9, No. 5-6, 2006, pp. 676-683, <https://doi.org/10.1016/j.crci.2005.02.042>.
- [6] G. Ramanathan, K. R. Murali, Photocatalytic Activity of  $\text{SnO}_2$  Nanoparticles, *J. Appl. Electrochem.*, Vol. 52, 2022, pp. 849-859, <https://doi.org/10.1007/s10800-022-01676-z>.
- [7] J. H. Lee, Y. J. You, M. A. Saeed, S. H. Kim, S. H. Choi, S. Kim, S. Y. Lee, J. S. Park, J. W. Shim, Undoped tin Dioxide Transparent Electrodes for Efficient and Cost-Effective Indoor Organic Photovoltaics ( $\text{SnO}_2$  Electrode for Indoor Organic Photovoltaics), *NPG Asia Mater.*, Vol. 13, No. 43, 2021, pp. 1-10, <https://doi.org/10.1038/s41427-021-00310-2>.
- [8] Y. Kong, Y. Li, X. Cui, L. Su, D. Ma, T. Lai, L. Yao, X. Xiao, Y. Wang,  $\text{SnO}_2$  Nanostructured Materials Used as Gas Sensors for the Detection of Hazardous and Flammable Gases: A review, *Nano Materials Science*, Vol. 4, No. 4, 2022, pp. 339-350, <https://doi.org/10.1016/j.nanoms.2021.05.006>.
- [9] R. Ponte, E. Rauwel, P. Rauwel, Tailoring  $\text{SnO}_2$  Defect States and Structure: Reviewing Bottom-Up Approaches to Control Size, Morphology, Electronic and Electrochemical Properties for Application in Batteries, *Materials*, Vol. 16, No. 12, 2023, <https://doi.org/10.3390/ma16124339>.
- [10] B. D. Cullity, S. R. Stock, Elements of X-Ray Diffraction, 3<sup>rd</sup> Ed., Prentice-Hall Inc., ISBN 0-201-61091-4.2001, pp. 96-102.
- [11] W. L. Bragg, The Reflection of X-rays by Crystals, *Proceedings of the Royal Society of London, Series A*, Vol. 89, No. 611, 1913, pp. 482-493.
- [12] N. Haddad, Z. B. Ayadi, H. Mahdhi, K. Djessas, Influence of Fluorine Doping on the Microstructure, Optical and Electrical Properties of  $\text{SnO}_2$  Nanoparticles, *J. Mater. Sci.: Mater. Electron.*, Vol. 28, 2017, pp. 15457-15465, <https://doi.org/10.1007/s10854-017-7433-1>.
- [13] J. Zuo, C. Xu, X. Liu, C. Wang, C. Wang, Y. Hu, Y. Qian, Study of the Raman Spectrum of Nanometer  $\text{SnO}_2$ , *J. Appl. Phys.*, Vol. 75, No. 3, 1994, pp. 1835-1836, <https://doi.org/10.1063/1.356348>.
- [14] S. Sambasivam, I. M. Obaidat, Effect of Iron Doping on ESR and Raman Spectra of  $\text{SnO}_2$  Nanomaterials, *Materials Today: Proceedings*, Vol. 28, 2020, pp. 587-590, <https://doi.org/10.1016/j.matpr.2019.12.225>.
- [15] N. Ahmad, S. Khan, M. M. N. Ansari, Exploration of Raman Spectroscopy, Dielectric and Magnetic Properties of (Mn, Co) Co-doped  $\text{SnO}_2$  Nanoparticles, *Phys. Rev. B Condens. Matter.*, Vol. 558, 2019, pp. 131-141, <https://doi.org/10.1016/j.physb.2019.01.044>.
- [16] S. Roy, A. G. Joshi, S. Chatterjee, A. K. Ghosh, Local Symmetry Breaking in  $\text{SnO}_2$  Nanocrystals with Cobalt Doping and Its Effect on the Optical Properties, *Nanoscale*, Vol. 10, No. 22, 2018, pp. 10664-10682, <https://doi.org/10.1039/C7NR07427A>.
- [17] L. Abello, B. Bochu, A. Gaskov, S. Koudryavtseva, G. Lucaleau, M. Roumyantseva, Structural Characterization of Nanocrystalline  $\text{SnO}_2$  by X-Ray and Raman Spectroscopy, *J. Solid State Chem.*, Vol. 135, No. 1, 1998, pp. 78-85, <https://doi.org/10.1006/jssc.1997.7596>.
- [18] N. Bhardwaj, S. Kuriakose, S. Mohapatra, Structural and Optical Properties of  $\text{SnO}_2$  Nanotowers and Interconnected Nanowires Prepared by Carbothermal Reduction Method, *J. Alloys Compd.*, Vol. 592, No. 15, 2014, pp. 238-243, <https://doi.org/10.1016/j.jallcom.2013.12.268>.

- [19] W. B. H. Othmen, B. Sieber, H. Elhouichet, A. Addad, B. Gelloz, M. Moreau, S. Szunerits, R. Boukherroub, Effect of High Fe Doping on Raman Modes and Optical Properties of Hydrothermally Prepared SnO<sub>2</sub> Nanoparticles, Materials Science in Semiconductor Processing, Vol. 77, 2018, pp. 31-39, <https://doi.org/10.1016/j.mssp.2017.12.014>.
- [20] V. Bonu, A. Das, A. K. Sivadasan, A. K. Tyagi, S. Dhara, Invoking Forbidden Modes in SnO<sub>2</sub> Nanoparticles Using Tip Enhanced Raman Spectroscopy, J. Raman Spectrosc, Vol. 46, No. 11, 2015, pp. 1037-1040, <https://doi.org/10.1002/jrs.4747>.
- [21] A. Diéguez, A. R. Rodríguez, A. Vilà, J. R. Morante, The Complete Raman Spectrum of Nanometric SnO<sub>2</sub> Particles. J. Appl. Phys., Vol. 90, No. 3, 2001, pp. 1550-1557, <https://doi.org/10.1063/1.1385573>.
- [22] R. Mani, K. Vivekanandan, K. Vallalperuman, Synthesis of Pure and Cobalt (Co) Doped SnO<sub>2</sub> Nanoparticles and its Structural, Optical and Photocatalytic Properties, J Mater Sci: Mater Electron, Vol. 28, No. 5, 2017, pp. 4396-4402, <https://doi.org/10.1007/s10854-016-6067-z>.
- [23] M. Xu, X. Ruan, J. Yan, Z. Zhang, J. Yun, W. Zhao, T. Li, Y. Shi, Synthesis, Growth Mechanism, and Photoluminescence Property of Hierarchical SnO<sub>2</sub> Nanoflower-rod Arrays: an Experimental and First Principles Study, J. Mater. Sci., Vol. 51, No. 21, 2016, pp. 9613-9624, <https://doi.org/10.1007/s10853-016-0169-0>.
- [24] H. Sefardjella, B. Boudjema, A. Kabir, G. Schmerber, Structural and Photoluminescence Properties of SnO<sub>2</sub> Obtained by Thermal Oxidation of Evaporated Sn Thin Films, Current Applied Physics, Vol. 13, No. 9, 2013, pp. 1971-1974, <https://doi.org/10.1016/j.cap.2013.08.017>.
- [25] I. L. P. Raj, M. S. Revathy, A. J. Christy, N. Chidhambaran, V. G. S. AlFaify, Study on the Synergistic Effect of Terbium-doped SnO<sub>2</sub> Thin Film Photocatalysts for Dye Degradation, J. Nanopart. Res., Vol. 22, No. 359, 2020, <https://doi.org/10.1007/s11051-020-05084-2>.